The Variability of the Horizontal Circulation in the Troposphere and Stratosphere - A Comparison

Judith Perlwitz

NASA/Goddard Institute for Space Studies, and Center for Climate
Systems Research, Columbia University, New York, USA

Hans-F. Graf

Max-Planck-Institute for Meteorology, Hamburg, Germany

11 Figures

Corresponding Address:
Judith Perlwitz
Center for Climate Systems Research
Columbia University/NASA-GISS
2880 Broadway
New York, NY, 10025
USA

Phone: +1 212 678 5592
Fax: +1 212 678 5552

email: judith@giss.nasa.gov

Summary

The variability of the horizontal circulation in the stratosphere and troposphere of the Northern Hemisphere (NH) is compared by using various approaches. Spatial degrees of freedom (dof) on different time scales were derived. Modes of variability were computed in geopotential height fields at the tropospheric and stratospheric pressure levels by applying multivariate statistical approaches. Features of the spatial and temporal variability of the winterly zonal wind were studied with the help of recurrence and persistence analyses. The geopotential height and zonally-averaged zonal wind at the 50-, 500- and 1000-hPa level are used to investigate the behavior of the horizontal circulation in the lower stratosphere, mid-troposphere and at the near surface level, respectively. It is illustrated that the features of the variability of the horizontal circulation are very similar in the mid-troposphere and at the near surface level. Due to the filtering of tropospheric disturbances by the stratospheric and upper tropospheric zonal mean flow, the variability of the stratospheric circulation exhibits less spatial complexity than the circulation at tropospheric pressure levels. There exist enormous differences in the number of degrees of freedom (or free variability modes) between both atmospheric layers. Results of the analyses clearly show that the concept of a zonally symmetric AO with a simple structure in the troposphere similar to the one in the stratosphere is not valid. It is concluded that the spatially filtered climate change signal can be detected earlier in the stratosphere than in the mid-troposphere or at the near surface level.

1 Introduction

During winter, the troposphere and middle atmosphere (strato- and meso-sphere) are closely coupled by dynamic processes. Wave motions in the middle atmosphere are primarily produced and maintained by the vertical propagation of gravity modes and Rossby modes which are both forced in the troposphere. Gravity waves explain only a small part of the total variability of the horizontal flow in the troposphere and stratosphere, in the mesosphere they often appear to be the dominant modes. The atmospheric flow in the troposphere shows a broad spectrum of Rossby modes, including synoptic scale waves, whereas the atmospheric flow in the middle atmosphere is mainly characterized by ultra-long planetary waves. The reason for this difference is that the zonal wind distribution in the middle atmosphere has a strong filtering effect on tropo-spheric disturbances as indicated by the Charney-Drazin Theorem (Charney and Drazin, 1961). Only ultra-long planetary Rossby waves are able to propa-gate into the middle atmosphere. The propagation time of these waves from the mid-troposphere into the stratosphere amounts to about a few days (Randel, 1988; Cheng and Dunkerton, 1995; Perlwitz and Graf, 2001). As a consequence of the filtering effect, the space-time variability of the horizontal circulation may differ between the troposphere and stratosphere especially at the time scale of high frequencies (e.g. days).

On the other hand, observational data and experiments with atmospheric general circulation models indicate a slow downward propagation of zonal wind anomalies from the mesosphere into the troposphere through the interaction of the upward propagating waves with the mean flow (Kodera et al., 1996; Kuroda and Kodera, 1999; Baldwin and Dunkerton, 1999). Because of this downward influence, we may expect similar behavior of the zonal mean flow in the troposphere and stratosphere on the time-scale of low frequencies (e.g. monthly means).

Empirical orthogonal function (EOF) analysis is a common approach to isolate modes of variability of the atmospheric circulation. The spatial struc-ture of the leading EOFs of the Northern Hemisphere's (NH) 50-hPa geopoten-tial height fields calculated on the basis of monthly means is similar to zonal harmonics. The first EOF is characterized by variations in the strength of the stratospheric polar winter vortex (Wallace et al., 1995; Perlwitz and Graf, 1995; Kodera et al., 1996). The leading EOFs of mid-tropospheric geopotential heights exhibit more complex hemispheric-scale structures (e.g., Wallace and Gutzler, 1981). The study of Thompson and Wallace (1998) emphasized the importance of the first EOF of sea level pressure (SLP). This mode, called Arc-tic Oscillation (AO), exhibits a quasi-zonally symmetric structure similar to the leading mode of circulation in the lower stratosphere (Thompson and Wallace, 1998).

Spatial patterns derived from EOF analysis are the most efficient patterns for explaining the temporal variance integrated over the entire analysis domain within the constraints of being both spatially and temporally orthogonal to each other. However, the pattern that represents variance most efficiently does not necessarily have anything to do with the underlying dynamic structure. Studying the coupled modes of variability of tropospheric and stratospheric cir-

culation increases the physical reliability of these modes because of the close dynamic coupling between both atmospheric layers (Perlwitz et al., 2000). Singular value decomposition (SVD) analysis and canonical correlation analysis (CCA) were used to isolate the coupled modes in the NH's 50- and 500-hPa height fields for winter means (Baldwin et al., 1994) and single winter months (Perlwitz and Graf, 1995).

Recently a debate arose about the physical nature of the AO (Corti et al., 1999; Monahan et al. 2001; Palmer, personal communication) versus the North Atlantic Oscillation (NAO). Here, we contribute to this discussion by comparing the variability and its structure of the horizontal circulation in the NH troposphere and stratosphere at different time scales. For this review, various approaches were applied. Spatial degrees of freedom (dof) were derived. Modes of variability were computed by applying multivariate statistical approaches. Features of the spatial and temporal variability of the winterly zonal wind were studied with the help of recurrence and persistence analyses. The 50-, 500- and 1000-hPa geopotential heights zonal wind fields used for this study were based on the National Centers for Environmental Prediction-National Center for Atmospheric Research (NCEP-NCAR) reanalysis (Kalnay et al., 1996). The data were obtained from the National Oceanic and Atmospheric Administration (NOAA) Climate Diagnostics Center (CDC). The time period from 1958 to 1999 was analyzed.

The number of dof is a parameter for describing the dimensionality of a dynamic system, such as the atmosphere, or for defining the number of independent variables in a dataset. Numerous studies exist using different approaches to estimate the dof of the NH tropospheric circulation (e.g., Fraedrich et al., 1995; Toth, 1995; Wang and Shen, 1999). Dof of the horizontal circulation in the lower stratosphere have not been investigated so far. Here, we will compare the spatial dof of the NH 50-, 500- and 1000-hPa geopotential heights on different time scales both for the summer and winter season (Section 2).

In section 3, we will discuss the modes of variability of NH geopotential height fields which were isolated with the EOF analysis and SVD analysis. Analogous to previous studies (Thompson and Wallace, 1998; Fyfe et al., 1999), the cold-season months November to April were analyzed.

Regime-like behavior of the atmospheric flow is manifested by the recurrence or persistence of flow patterns (Wallace et al., 1991; Dole and Gordon, 1983). Both features of the zonally-averaged zonal wind $\bar{u}$ were studied in order to compare time-space anomaly structures of $\bar{u}$ at the 50-, 500- and 1000-hPa level in the winter season (Section 4).

2 Spatial Degrees of Freedom of the Atmospheric Flow

We used the simplified method of Fraedrich et al. (1995) to compare the complexity of the horizontal circulation between the troposphere and stratosphere. The estimate is based on a linear approach, because spatial patterns are described in terms of EOFs. The spatial dof are estimated by comparing the variance of the theoretical standardized chi-squared distribution with the sum

of the squared eigenvalues of a spatial correlation matrix:

$$dof = N^2 / \sum_{k=1}^{N} \lambda_k^2 \qquad (1)$$

where N is the number of grid-points and λ_k is the kth eigenvalue of the correlation matrix.

Our estimates of the spatial dof of the NH stratospheric and tropospheric flow are based on grid-point data of the 50-, 500-hPa and 1000-hPa geopotential heights north of 30°N. We analyzed unfiltered daily data, low-pass (> 10-days) filtered daily data and monthly means. Low-pass filtered daily data were determined on the basis of the 21-point filter by Blackmon and Lau (1980). By using this filtering, synoptic scale disturbances (< 10 days) are removed. Before applying EOF analysis, the data were transformed from a regular $5° \times 5°$ grid to an equal-area grid in order to avoid an overestimation of the variability at high latitudes.

Table 1 shows the dof calculated for both the summer (June to August, JJA) and the winter (December to February, DJF) seasons. The tropospheric dof agree well with published results. For example, Wallace et al. (1991) calculated 20 dof for the NH low-pass filtered daily 500-hPa geopotential heights for winter. The dof of the unfiltered 1000-hPa heights are consistent with the results of Fraedrich et al. (1995) taking into account that they analyzed data of a smaller region (30° - 75°N). The estimates of Fraedrich et al. (1995) amount to about 21 dof for January and about 32 dof for July. Our analysis indicates that for the winter season the dof for the near surface geopotential heights (Z_{1000}) are nearly equal to the mid-tropospheric dof (Table 1). The increase from the winter to the summer season, however, is somewhat smaller at the near surface level than at the 500-hPa level.

The interseasonal variation in the number of independent circulation modes at tropospheric pressure levels is consistent with the finding that regime-like behavior is less present during summer than during winter (Wallace and Zhang, 1993). During the latter season, the tropospheric flow is dominated by large-scale dynamic processes like the generation of ultra-long planetary waves by orography and heat sources. During summer, local processes like convection play a more important role and the relative dominance of the large-scale dynamics is strongly reduced. The local processes may be more relevant for the circulation in the free troposphere than near the surface since the number of dof is smaller at the 1000-hPa level than at the 500-hPa level.

Comparing the troposphere with the lower stratosphere (Z_{50}), we found that the stratospheric flow is characterized by a considerably smaller number of spatial dof (Table 1). The reason is that only ultra-long planetary scale motions can be observed in the stratosphere. Further reduction of the dof is relatively small in the stratosphere, when low-pass filtered variability or monthly averaged fields are studied, since synoptic-scale Rossby waves are strongly trapped in the troposphere. In addition, the troposphere and stratosphere exhibit different interseasonal behavior. In contrast to the troposphere, in the stratosphere the number of dof decreases form winter to summer. The reason for this decrease is that the dynamic coupling between troposphere and stratosphere is very weak during summer. Tropospheric disturbances cannot propagate into the

stratosphere characterized by an easterly zonal mean flow (Charney and Drazin, 1961). As a consequence, a stratospheric mean state which is close to the radiative equilibrium is observed during summer (Fels, 1985).

3   Modes of Variability

The main goal of this section is to compare the leading modes of variability of the NH horizontal circulation at different pressure levels (50-, 500- and 1000-hPa) for monthly mean data. First, the leading EOFs of the pressure fields are discussed (section 3.1). Then, the EOF analysis results are compared with the coupled modes of variability of the tropospheric and stratospheric geopotential height fields (section 3.2). SVD analyses were applied to calculate the coupled modes. With the help of this approach the patterns (singular patterns) are isolated which describe maximum covariance between two fields (Bretherton et al., 1992). The SVD analysis is a straightforward expansion of the EOF analysis and the local weights in the singular patterns and the EOFs can be compared.

The monthly means from November to April were analyzed. During this time of the year, on average, the zonally-averaged zonal wind at the 50-hPa level is westerly, and one standard deviation (σ) of monthly interannual variability in mid-latitude exceeds $2.5\,\mathrm{m\,s^{-1}}$ (Figure 1). Before applying the EOF and SVD analysis, the mean seasonal cycle and the long-term trends for each month were removed from the time series. The data were analyzed on a $5° \times 5°$ grid. The grid point data were weighted with the square root of the cosine of the latitude before determining the covariance matrix in order to use equal-area weighted data.

3.1   EOF Analysis Results

In Figure 2, the spectra of the first 9 eigenvalues of the 50-, 500- and 1000-hPa heights are shown together with their errorbars. We calculated the sampling errors of the eigenvalues according to North's Rule of Thumb (North et al., 1982). These errorbars indicate that the first three EOFs are well separated in both the stratospheric (Figure 2a) and the near surface field (Figure 2c). In the mid-tropospheric field (Figure 2b), the eigenvalues of the second and third modes are very close. Thus, it is quite probable that a linear combination of these two EOFs is also an EOF of this field.

The first three EOFs of the 50- and 500-hPa fields are displayed in Figures 3 and 4, respectively. The fraction of the total variance explained by the individual EOFs is given at the right upper corner of each EOF map. The first three EOFs of 1000-hPa heights being very similar to the respective patterns of the SLP (Fyfe et al., 1999, Plate 1) explain 20, 12 and 10% of the total variance in the domain north of 30°. A principal reason for the difference in the dimensionality of the horizontal flow in the troposphere and stratosphere, as illustrated with the help of spatial dof, becomes clear. At the stratospheric level, the leading EOF of the geopotential height field already describes a large fraction (about 50%) of the total variance. The first three EOFs taken together account for more than 74% of the total variance. The eigenvalue spectra of the 500- and

6

1000-hPa height fields exhibit a slow and more continuous drop (Figures 2b and 2c). To explain 75% of the total variance, the first 10 EOFs (500-hPa heights) and the first 9 EOFs (1000-hPa heights) have to be considered.

The EOFs of the 50-hPa field clearly assume the form of zonal harmonics because of the strongly reduced influence of longitudinal asymmetries in the lower boundary conditions (North, 1975; Wallace et al., 1995). The leading EOF of the stratospheric geopotential height field shows a circumpolar pressure seesaw between high and subpolar latitudes (Figure 3a). Thus, this EOF describes the variation in the strength of the polar winter vortex (Perlwitz and Graf, 1995; Kodera et al., 1996). Both the second and the third mode of the 50-hPa height field have the structure of waves of zonal wave number 1 (Figures 3b and 3c). The phase of the third EOF is shifted with respect to the phase of the second one by 90° at zonal direction. The next two higher modes (not shown) exhibit the structure of waves of zonal wave number 2. These two higher modes contribute significantly to the total variability, not on the basis of monthly means, but on the daily time scale.

In contrast, the EOFs of the 500-hPa geopotential height field exhibit more complex, global scale structures by forming wave trains. The first EOF shows a main center over southern Greenland. The mid-latitude centers of action with opposite sign appear over the North Pacific, the western Atlantic and Central Europe (Figure 4a). The second and third EOF (Figures 4b and 4c) show a similar wave train-like structure in which the centers of action of the third EOF appear near the nodelines between the centers of action of the second EOF. The second EOF is similar to the circulation pattern that corresponds to the cold-ocean-warm-land (COWL) temperature pattern which explains a large fraction of the temperature change observed during the recent decades (Wallace et al., 1996). The eigenvalue of this EOF is not clearly separated from the eigenvalue of the third EOF even when all 246 monthly realizations are used. However, this pattern is very robust when reanalysis data for a longer period (1949–1999) are studied (not shown). The positive phase of the second EOF of the 500-hPa flow (Figure 4b) exhibits a preferred regime determined on the basis of nonlinear approaches (Corti et al., 1999; Monahan et al., 2001). The first two EOFs shown in Figures 4a and 4b have a similar structure as the first two EOFs determined by Kimoto and Ghil (1993) using 10-day low-pass filtered 700-hPa geopotential heights. The EOFs of the 500-hPa geopotential heights differ from the results of Wallace and Gutzler (1981). Clearly, one reason is that Wallace and Gutzler (1981) investigated a smaller sample (December to February, 1962–1977) and may have analyzed another climate regime. Such differences can well appear as Perlwitz et al. (2000) showed in a model study. It is also highly relevant that the EOFs have been determined on the basis of the covariance matrix in the present study, whereas Wallace and Gutzler (1981) analyzed the correlation matrix which emphasizes the structural features more than amplitudes.

The first EOF of the 1000-hPa field (Figure 5) exhibits a more zonally symmetric structure than the first EOF of the 500-hPa field, with geopotential height perturbations of opposing signs in the polar cap region and in the surrounding zonal ring centered near 45°N (Thompson and Wallace, 1998). Even though the AO is often described as a zonally symmetric feature, the weights

of the EOFs (Figure 5) show asymmetries at midlatitudes along a zonal circle. The midlatitude part of the AO has distinct centers of action over the Northeast Atlantic and North Pacific. The second and third EOFs (not shown) exhibit similar local structures as the third and second EOFs of the 500-hPa field (Figures 4c and 4b), respectively.

3.2   Coupled Modes of Variability

The leading EOFs are patterns which describe maximum variance; they are not necessarily selected for physical reasons. Studying the coupled modes between the time series of two fields for which a physically determined interaction is theoretically established may increase the physical relevance of these modes (Baldwin et al., 1994; Perlwitz and Graf, 1995; Perlwitz et al., 2000). Two SVD analyses were carried out using the 50-hPa height field as one dataset and the 500- and 1000-hPa height fields as the second dataset, respectively. The results (spectrum of eigenvalues and 50-hPa singular patterns) agree very well between both analyses.

In Figure 6, the spectrum of eigenvalues of the cross-covariance matrix between the time series of the 500- and 50-hPa height is shown together with their errorbars. This spectrum indicates that not only the first, but also the second coupled variability mode can be very well separated from the next higher modes. The first and second coupled mode explain 64% and 15% of the total squared covariance, respectively.

Figures 7a and 7b show the singular patterns of the first coupled mode of variability in the 50- and 500-hPa height fields. In addition, the 1000-hPa singular pattern of the SVD analysis in the 50- and 1000-hPa fields is given in Figure 7c. The respective patterns for the second coupled modes are displayed in Figure 8. Again, the fraction of total variance explained by the individual singular patterns is given at the upper right corner of each map. In contrast to the leading EOFs (Figures 3 and 4), the stratospheric and tropospheric patterns for each coupled mode show a stronger structural similarity, although the tropospheric patterns still appear more complex than the 50-hPa patterns. Clearly, the explained fraction of total variance is smaller for the singular patterns than for the EOF.

For the first coupled mode, the structural differences between the 50-hPa singular pattern (Figure 7a) and the first EOF (Figure 3a) are small and only appear at mid-latitudes over western Europe and the North Pacific. The differences in the respective patterns of the 500-hPa field are more pronounced (Figures 7b and 4a). The main centers of action of the tropospheric singular pattern are found over the North Atlantic and over eastern Asia (Figure 7b). In contrast, the first EOF of this tropospheric field has - by definition - a more hemispheric-scale structure (Figure 4a) in which also the North Pacific is strongly involved. Similar differences can be found by comparing the respective singular pattern and the EOF for the 1000-hPa height field (Figures 7c and 5). This preferred coupled circulation mode exhibits the well-known close relationship between the strength of the stratospheric polar winter vortex and the strength of the westerlies over the North Atlantic in the troposphere (Baldwin et al., 1994; Perlwitz and Graf, 1995; Graf et al., 1995; Kodera et al., 1996; Baldwin and

8

Dunkerton, 1999). The studies by Deser (2000) and Perlwitz and Graf (1995) indicate that the temporal correlation between the strength of the stratospheric polar vortex and the circulation over the Pacific is not significant on the basis of the observations that are available. The first coupled mode mainly describes the downward influence from the stratosphere into the troposphere by the slow downward propagation of zonal mean wind anomalies through wave-mean flow interactions (Baldwin and Dunkerton, 1999; Kodera et al., 1999) that lead to a change in the meridional propagation of tropospheric waves (Limpasuvan and Hartmann, 2000; Perlwitz and Graf, 2001). The changes in the NH tropospheric and stratospheric circulation observed during the last 40 years show a similar spatial structure as the positive phase of the leading coupled mode (Graf et al., 1995; Kodera and Koide, 1997).

For the second coupled mode, the 50-hPa pattern exhibits a superposition of wave anomalies of zonal wave numbers 1 and 2 (Figure 8a). The related tropospheric pattern shows two wave trains (Figure 8b). Together, they exhibit a wave-like structure of zonal wave number 2 at higher latitudes (north of 60°N). At the near surface level, two separated centers of action with the same sign appear. They are found over the North Pacific and over northern Europe. This coupled mode evolves from the upward propagation of tropospheric quasi-stationary disturbances into the stratosphere (Randel, 1988; Cheng and Dunkerton, 1995; Perlwitz and Graf, 2001). The propagation time from the 500- to the 50-hPa level amounts to about 2 to 6 days. On the monthly time scale, an equivalent-barotropic increase with height of the anomalies over North America and Scandinavia appears.

The leading EOFs of the atmospheric circulation at the near surface level were used for the detection of anthropogenic climate changes (Fyfe et al., 1999; Shindell et al., 1999; Gillett et al., 2000). By using the coupled modes of tropospheric and stratospheric circulation instead of EOFs at single pressure levels, physical mechanisms would be more strongly included in the detection approach. Thus, the explained variance of the climate change signal may be higher using the coupled modes, although EOFs clearly explain more variance in the hemispheric-scale height fields.

4   Variability Characteristics of the Zonally-Averaged Zonal Wind

The AO as the leading EOF has received increased attention during recent years because of its strong tropospheric zonality which is similar to the leading EOF in the lower stratosphere (Thompson and Wallace, 1998). To compare the behavior of $\bar{u}$ at the tropospheric and stratospheric pressure levels in more detail, we applied the same methods used to study the regime-like behavior of low-frequency atmospheric flow (Wallace et al., 1991; Dole and Gordon, 1983). Regime-like behavior of atmospheric flow is manifested by recurrence or persistence of flow patterns. We studied these features in the NH ($\bar{u}$) at the 50-, 500- and 1000-hPa pressure level. The $\bar{u}$ north of 30°N is used. The latitudinal distance between two adjacent zonally-averaged values amounts to 2.5°.

4.1 Recurrence of Anomaly Patterns

The anomaly patterns of $\bar{u}$ at specific pressure levels are one-dimensional arrays. We calculated the frequency distribution of spatial correlation between these anomaly patterns (referred to as anomaly correlation) based on a large number of pairs of the low-pass filtered arrays of $\bar{u}$. The analyses were performed for mid-winter months (DJF) for the period from December 1958 to February 1999. We removed the climatological annual cycle before applying the temporal filtering. From the filtered time series, arrays at 5-day intervals, i.e., a total of 738 arrays (18 graphs × 41 years) were selected. Following the approach used by Gutzler and Shukla (1984) and Wallace et al. (1991), we calculated the anomaly correlation r_{ij} between two graphs $\bar{u}_i$ and $\bar{u}_j$

$$r_{ij} = \frac{[(\bar{u}_i - \bar{u}_i^g)(\bar{u}_j - \bar{u}_j^g)]}{\sqrt{[(\bar{u}_i - \bar{u}_i^g)^2]}\sqrt{(\bar{u}_j - \bar{u}_j^g)^2}}, \tag{2}$$

where $\bar{u}^g$ is the spatial mean, the indices i and j identify particular arrays, and the brackets operator [ ] represents an average over all grid points. Pairs of graphs with large positive anomaly correlation may reflect circulation regimes that recur relatively frequently within the time period studied. Only half of the 738×737 matrix need to be computed since $r_{ij} = r_{ji}$. The frequency distribution of the anomaly correlations was determined on the basis of the correlation coefficients between all graphs excluding those from the same winter.

Figure 9 shows the frequency distributions of these anomaly correlations at the 50-, 500- and 1000-hPa levels. The frequency distribution of $\bar{u}_{50}$ exhibits a strong bimodality (Figure 9a). The most frequent correlation coefficients occur in the classes from 0.8 to 0.9, and from -0.9 to -0.8. Thus, the variability of $\bar{u}_{50}$ has one preferred latitudinal structure appearing in its two polarities. In contrast, the corresponding frequency distributions of the $\bar{u}_{500}$ and $\bar{u}_{1000}$ have one broad maximum region centered between -0.6 and 0.6 where values larger than 15000 occur (Figure 9b and 9c). We repeated the analysis for monthly means in order to stress on the time scale of lower frequencies and found similar results as for daily data.

The frequency distributions of $\bar{u}$ can be understood within the context of the non-linear paradigm for the description of low-frequency variability (Wallace et al., 1991, for a review). This non-linear paradigm views the climatological mean as an arbitrary mathematical construct, which does not need to bear any relation to the most frequently observed state(s) of the atmosphere. It predicts that indices of spatial patterns may exhibit highly skewed or even bi- (or multi-) modal frequency distributions. The bimodal distribution of the anomaly correlations of $\bar{u}$ in the stratosphere exhibits such non-linear behavior (Figure 9a). The two patterns, which belong to the maxima, exhibit an anomalously strong and weak polar winter vortex with maximum anomalies between 55° and 75°N. The lack of uni- or bimodality in the mid-troposphere as indicated by Figure 9b is helped by the presence of a large number of waves of different wave numbers, allowing for multiple non-linear interactions amongst them, and hence a variety of patterns. In addition, the $\bar{u}_{500}$ and $\bar{u}_{1000}$ fields, which completely smooth the longitudinal structures of circulation, are insufficient for the understanding of tropospheric flow regimes. A non-linear approach, however, gave indications for

10

preferred flow regimes in the hemispheric-scale height fields (Corti et al., 1999; Monahan et al., 2001).

To highlight the importance of the anomaly strength, we also calculated the frequency distribution of the spatial covariance between pairs of arrays. We found that strong bimodality in $\bar{u}_{50}$ is only a feature of the anomaly correlation, i.e., it does not result from the strength of the anomaly, but rather clearly reflects structural effects. Further evidence of the nonlinearities in the stratosphere is given by the study of Gillett et al. (2001). They showed that the index of the AO in the stratosphere is negatively skewed in the winter and positively skewed in the spring. Histograms of the polar temperature at the 70-hPa level show the opposite skewness to those of the AO index.

4.2 Persistence of the Leading EOF

The previous analysis (section 4.1) has not given any information about the persistence of a specific structure that very often appears in its two polarities (e.g., anomalously strong and anomalously weak polar winter vortex). We studied this behavior in more detail on the basis of 10-day low-pass filtered time series of $\bar{u}$. We determined the leading EOF of $\bar{u}$ at the 50-, 500- and 1000-hPa level for the winter months (December to February). Again, the data were weighted with the cosine of the latitude and the climatological annual cycle was removed before applying EOF analysis. The EOFs were derived on the basis of the covariance matrix.

The first EOF of $\bar{u}_{50}$, $\bar{u}_{500}$ and $\bar{u}_{1000}$ are shown in Figure 10. The corresponding explained fractions of the total variance are 71%, 40% and 36%, respectively. The first stratospheric EOF describes the variation in the strength of the stratospheric polar winter vortex, with a maximum variation around 65°N. Corresponding to earlier findings (Branstator, 1984), the leading EOF of the tropospheric fields exhibits the typical shift in the tropospheric jets.

We determined the positive and negative persistence of these two patterns by using the standardized temporal expansion coefficients, i.e. the mean value and the standard deviation (σ) are equal to zero and one, respectively. Anomalies larger than the absolute value of 0.5σ are defined as relevant anomalies. We studied the duration (e.g., longer than 10 days) of relevant positive and negative anomalies. These events, determined for each 90-day period of the 41 years considered, were counted for specific durations. The total number was normalized to a 10-year period. We found that the distributions of the events for positive and negative anomalies were very similar. The total sum of events is shown in Figure 11. It can be seen that the tropospheric indices drop faster with increasing duration than the stratospheric index. A persistence of 40 days or more of relevant anomalies ($> 0.5\sigma$ or $< -0.5\sigma$), which have the pattern of the leading EOFs, is observed only once in the troposphere and 4 times in the lower stratosphere within 10 years.

The remarkable persistence of an anomalously strong or weak stratospheric polar vortex results from a positive feedback mechanism that exists between the wave forcing of the zonal-mean flow and the refraction of Rossby waves by the mean flow. The propagation of wave energy into the polar stratosphere, which occurs in conjunction with weaker lower stratospheric winds, results in

11

a stronger wave forcing of the mean winds in the stratosphere. The wave drag tends to maintain the weak winds and, therefore, a warm polar stratosphere, that allows a continuous strong propagation of waves into the stratosphere. On the other hand, strong lower stratospheric winds shield the polar stratosphere from wave activity and allow it to more closely approach the radiative equilibrium state.

Thus, due to the positive feedback mechanism of wave–mean flow interaction, an anomalously weak or strong polar stratospheric vortex, caused by an external forcing or internal variability, is maintained for longer periods. However, Figure 11 indicates that the effect of such positive feedback mechanisms is limited. On the one hand, the persistence of an anomalously weak vortex requires a continuous influx of wave activity from the troposphere which is not given at all instances. On the other hand, sudden warmings resulting from anomalous tropospheric conditions destroy the cold, anomalously strong polar vortex. Kodera et al. (2000) showed that a stronger polar vortex state is not always stationary. It slowly propagates, and sudden warmings occur in phase with this slow variability.

In contrast, the $\bar{u}$ at the 500-hPa and the 1000-hPa level does not show the features described for the 50-hPa level. The reason is that numerous processes affect a wide variety of mid-tropospheric circulation patterns. Such processes are the generation of large-scale Rossby waves by diabatic heating and orography, the generation of baroclinic and barotropic instabilities, interaction of large-scale and synoptic scale disturbances, and air-sea interaction. This all strongly affects the relatively small persistence or lack of stability of specific patterns of the tropospheric circulation. The stratosphere receives energy from these disturbances, but these are strongly filtered spatially. Such disturbances cannot be produced in the stratosphere itself.

5 Conclusions

To compare the variability of the horizontal circulation in the stratosphere and troposphere in the NH, various approaches were used such as estimating the spatial dof, isolating the modes of variability and studying features of the zonal mean flow by applying persistence and recurrence analyses. The geopotential height and zonally-averaged zonal wind at the 50-, 500- and 1000-hPa level were used to investigate the behavior of the horizontal circulation in the lower stratosphere, mid-troposphere and at the near surface level, respectively.

Our analyses illustrate that the features of the variability of the horizontal circulation at the near surface level and in the mid-troposphere are very similar, although planetary waves play a more important role in the mid-troposphere. Due to the filtering of tropospheric disturbances by the stratospheric mean zonal flow, the variability of the stratospheric circulation exhibits less spatial complexity than the circulation at tropospheric pressure levels. On the monthly mean time scale, variations in the zonal mean flow explain about 50% of the total variability of the stratospheric geopotential height fields. The number of spatial dof (or free variability modes) is much smaller in the stratosphere than in the troposphere. The results clearly show that the concept of a zonally symmetric AO with a simple structure in the troposphere similar to the one

in the stratosphere is not valid. Neither EOF analysis nor the leading coupled mode of the tropospheric and stratospheric circulation, determined with the help of SVD analysis, produce zonally symmetric patterns in the midlatitudes in the troposphere. Characteristic features of the variation in the zonally-averaged zonal wind strongly differ between both atmospheric layers.

An analysis of coupled variability modes of the tropospheric and stratospheric circulation together is able to more clearly elaborate on the physically based mechanisms of climate variability. However, the application of linearized methods like CCA and SVD still prevents the detection of non-linear changes and processes.

Since the stratospheric circulation, due to the strong filtering effect of the mean wind field on tropospheric disturbances, exhibits a much better signal to noise ratio, future climate change detection on the basis of modes of variability should incorporate more extensively the analyses of stratospheric phenomena. The spatially filtered climate change signal may be detected earlier in the stratosphere than in the mid-troposphere or at the near surface level. However, there is no reason to believe that the changes in the stratosphere would have a one-to-one projection onto the troposphere.

Acknowledgements

References

Baldwin, M. P. and T. J. Dunkerton, 1999: Propagation of the Arctic Oscillation from the stratosphere to the troposphere, *J. Geophys. Res.*, **104**, 30937–30946.

Baldwin, M. R., X. Cheng, and T. J. Dunkerton, 1994: Observed correlations between winter-mean tropospheric and stratospheric circulation anomalies, *Geophys. Res. Lett.*, **21**, 1141–1144.

Blackmon, M. L. and N. C. Lau, 1980: Regional characteristics of the Northern Hemisphere wintertime circulation: a comparison of the simulation of a GFDL general circulation model with observations, *J. Atmos. Sci.*, **37**, 497–514.

Branstator, G., 1984: The relationship between the zonal mean flow and quasi-stationary waves in the mid-troposphere, *J. Atmos. Sci.*, **41**, 2163–2178.

Bretherton, C. S., C. Smith, and J. M. Wallace, 1992: An intercomparision of methods for finding coupled patterns in climate data, *J. Clim.*, **5**, 541–560.

Charney, J. G. and P. G. Drazin, 1961: Propagation of planetary-scale disturbances from the lower into the upper atmosphere, *J. Geophys. Res.*, **66**, 83–109.

Cheng, X. and T. Dunkerton, 1995: Orthogonal rotation of spatial patterns derived from singular value decomposition analysis, *J. Clim.*, **9**, 2631–2643.

Corti, S., F. M. F, and T. N. Palmer, 1999: Signature of recent climate change in frequencies of natural atmospheric circulation regimes, *Nature*, **398**, 799–802.

Deser, C., 2000: On the teleconnectivity of the "Arctic Oscillation", *Geophys. Res. Lett.*, **27**, 779–782.

Dole, R. M. and N. D. Gordon, 1983: Persistent anomalies of the extratropical Northern Hemisphere wintertime circulation: Geographical distribution and regional persistence characteristics, *Mon. Wea. Rev.*, **111**, 1567–1586.

Fels, S. B., 1985: Radiative-dynamical interactions in the middle atmosphere, *Advances in Geophysics*, **A28**, 277–300.

Fraedrich, K., C. Ziehmann, and F. Sielmann, 1995: Estimation of spatial degrees of freedom, *J. Clim.*, **8**, 361–369.

Fyfe, J. C., G. J. Boer, and G. M. Flato, 1999: The Arctic and Antarctic Oscillations and their projected changes under global warming, *Geophys. Res. Lett.*, **26**, 1601–1604.

Gillett, N. P., M. P. Baldwin, and M. R. Allen, 2001: Evidence for nonlinearity in observed stratospheric circulation changes, *J. Geophys. Res., in press*.

Gillett, N. P., G. C. Hegerl, M. R. Allen, and P. A. Stott, 2000: Implications of changes in the Northern Hemisphere circulation for the detection of anthropogenic climate change, *Geophys. Res. Lett.*, **27**, 993–996.

Graf, H.-F., J. Perlwitz, I. Kirchner, and I. Schult, 1995: Recent northern winter climate trends, ozone changes and increased greenhouse gas forcing, *Contr. Atm. Phys.*, **68**, 233–248.

Gutzler, D. S. and L. Shukla, 1984: Analogs in the wintertime 500-mb height field, *J. Atmos. Sci.*, **41**, 177–189.

Kalnay, E., M. Kanamitsu, R. Kistler, W. Collins, D. Deaven, L. Gandin, M. Iredell, S. Saha, G. White, J. Woollen, Y. Zho, A. Leetmaa, R. Reynolds, M. Chelliah, W. Ebisuzaki, W. Higgins, J. Janowiak, K. C. Mo, C. Ropelewski, J. Wang, R. Jenne, and D. Joseph, 1996: The NCEP/NCAR 40-year reanalysis project, *B. Am. Meteorol. Soc.*, **77**, 437–471.

Kimoto, M. and M. Ghil, 1993: Multiple flow regimes in the Northern Hemisphere winter: Part I: Methodology and hemispheric regimes, *J. Atmos. Sci.*, **50**, 2625–2643.

Kodera, K., M. Chiba, H. Koide, A. Kitoh, and Y. Nikaidou, 1996: Interannual variability of the winter stratosphere and troposphere, *J. Meteor. Soc. Japan*, **74**, 365–382.

Kodera, K. and H. Koide, 1997: Spatial and seasonal characteristics of recent decadal trends in the northern hemispheric troposphere and stratosphere, *J. Geophys. Res.*, **102**, 19433–19447.

Kodera, K., K. Koide, and H. Yoshimura, 1999: Northern hemisphere winter circulation associated with the North Atlantic Oscillation and stratospheric polar-night jet, *Geophys. Res. Lett.*, **26**, 443–446.

Kodera, K., Y. Kuroda, and S. Pawson, 2000: Stratospheric sudden warmings and slowly propagating zonal-mean zonal wind anomalies, *J. Geophys. Res.*, **105**, 12351–12359.

Kuroda, K. and K. Kodera, 1999: Role of planetary waves in the stratosphere-troposphere coupled variability in the Northern Hemisphere winter, *Geophys. Res. Lett.*, **26**, 2375–2378.

Limpasuvan, V. and D. L. Hartmann, 2000: Wave-maintained annular modes of climate variability, *J. Clim.*, **13**, 4414–4429.

Monahan, A. H., L. Pandolfo, and J. C. Fyfe, 2001: The preferred structure of variability of the Northern Hemisphere atmospheric circulation, *Gephys. Res. Lett. in press*.

North, G. R., 1975: Theory of energy-balance climate models, *J. Atmos. Sci.*, **32**, 2033–2043.

North, G. R., T. L. Bell, R. F. Cahalan, and F. J. Moeng, 1982: Sample errors in the estimation of empirical orthogonal functions, *Mon. Wea. Rev.*, **110**, 699–707.

Perlwitz, J. and H.-F. Graf, 1995: The statistical connection between tropospheric and stratospheric circulation of the Northern Hemisphere in winter, *J. Clim.*, **8**, 2281–2295.

Perlwitz, J. and H.-F. Graf, 2001: Troposphere-stratosphere dynamic coupling under strong and weak polar vortex conditions, *J. Geophys. Res.*, **28**, 271–274.

Perlwitz, J., H.-F. Graf, and R. Voss, 2000: The leading mode of the coupled troposphere-stratosphere winter circulation in different climate regimes, *J. Geophys. Res.*, **105**, 6915–6926.

Randel, W. J., 1988: Further modification of time-longitude lag-correlation diagrams: Application to three-dimensional wave propagation, *Tellus*, **40A**, 257–271.

Shindell, D. T., R. L. Miller, G. A. Schmidt, and L. Pandolfo, 1999: Greenhouse gas forcing of Northern Hemisphere winter climate trends, *Nature*, **399**, 452–455.

Thompson, D. W. J. and J. M. Wallace, 1998: The Arctic Oscillation signature in the wintertime geopotential height and temperature fields., *Geophys. Res. Lett.*, **25**, 1297–1301.

Toth, Z., 1995: Degrees of freedom in Northern Hemisphere circulation data, *Tellus*, **47**, 457–472.

Wallace, J. M., X. Chen, and D. Sun, 1991: Does low-frequency atmospheric variability exhibit regime like behavior?, *Tellus*, **43**, 16–26.

Wallace, J. M. and D. S. Gutzler, 1981: Teleconnections in the geopotential height field during the Northern Hemisphere winter, *Mon. Wea. Rev.*, **109**, 784–812.

Wallace, J. M. and Y. Zhang, 1993: Structure and seasonality of interannual and interdecadal variability of the geopotential height and temperature fields in the Northern Hemisphere troposphere, *J. Clim.*, **6**, 2063–2082.

Wallace, J. M., Y. Zhang, and L. Bajuk, 1996: Interpretation of interdecadal trends in Northern Hemisphere surface air temperature, *J. Clim.*, **9**, 249–259.

Wallace, J. M., Y. Zhang, and J. A. Renwick, 1995: Dynamic contribution to hemispheric mean temperature trends, *Science*, **270**, 780–783.

Wang, X. and S. S. Shen, 1999: Estimation of spatial degrees of freedom of a climate field, *J. Clim.*, **12**, 1280–1291.

Table 1: Estimates of the spatial degrees of freedom (dof) for the horizontal flow at the 50-, 500- and 1000-hPa levels (north of 30°N). Results are shown for the winter season (DJF) and the summer season (JJA) using daily data, low-pass ($>$ 10-days) filtered daily data and monthly means.

	daily		daily (low-pass)		monthly	
	DJF	JJA	DJF	JJA	DJF	JJA
Z_{50}	9	4	8	3	5	2
Z_{500}	29	46	21	36	13	19
Z_{1000}	29	37	20	27	13	15
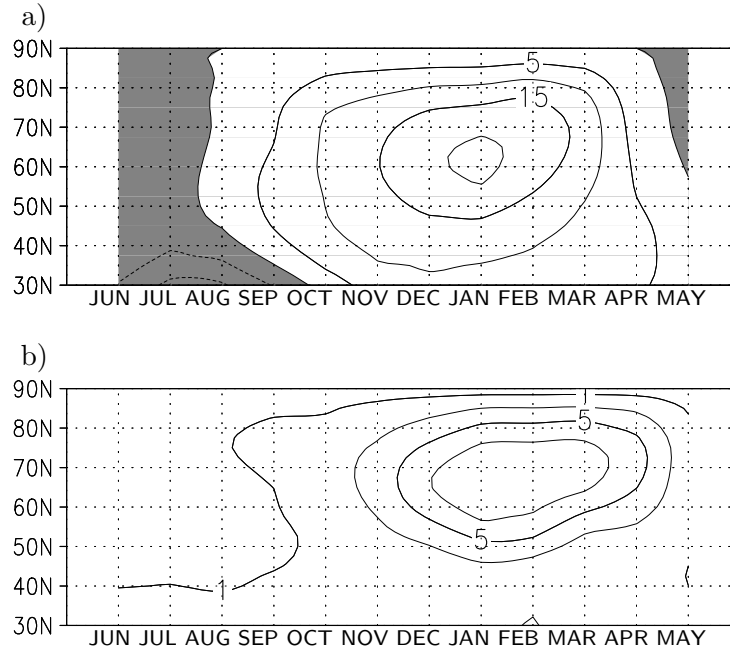
Figure 1: a) Long-term monthly mean and (b) monthly standard deviation of the zonally-averaged zonal wind at 50-hPa in [m s^{-1}]. Negative values in (a) are shaded. The contour intervals are 5 m s^{-1} in (a) and 2.5 m s^{-1} in (b).

17
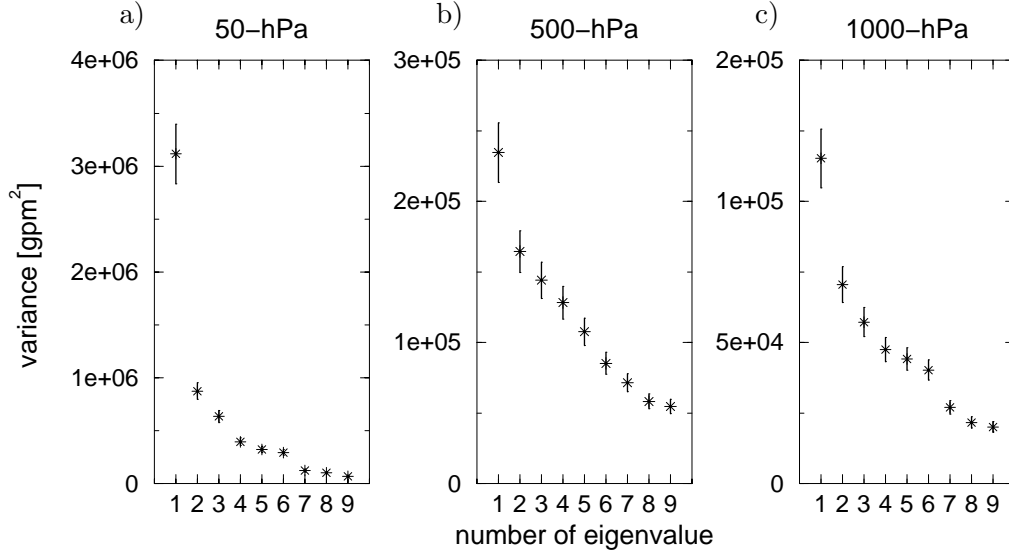
Figure 2: Eigenvalues and errorbars for the first 10 EOFs of the a) 50-hPa, b) 500-hPa and c) 1000-hPa geopotential height fields. The errorbars of the eigenvalues were calculated according to North et al. (1982).
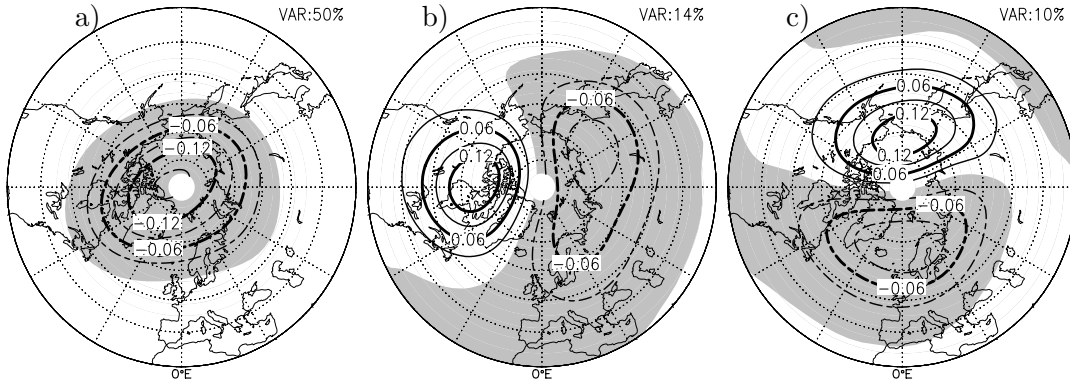
Figure 3: a) First, b) second and c) third EOF of the 50-hPa NH (north of 30°N) geopotential height field. Negative values are shaded. The fraction of explained total variance is given at the upper right corner of the individual maps.
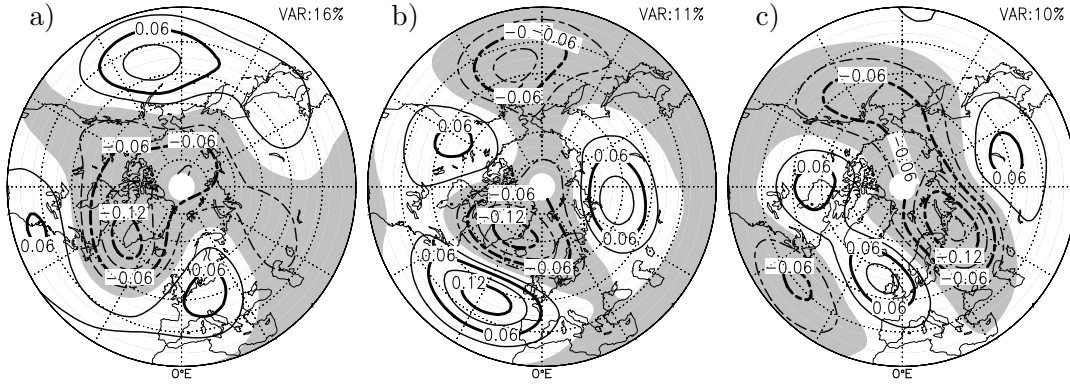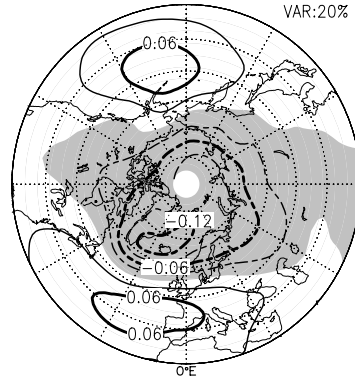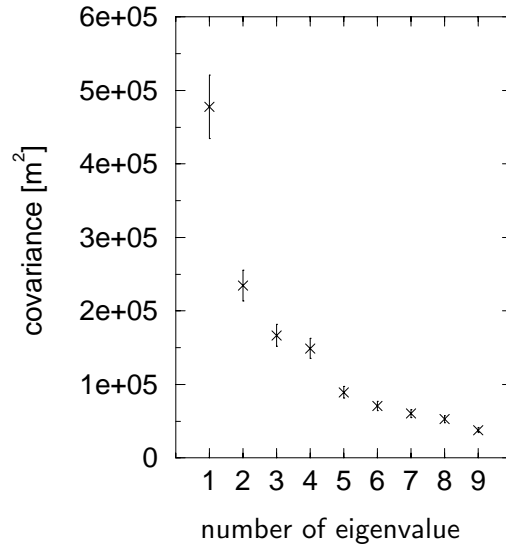
Figure 4: Same as Figure 3, but for the 500-hPa geopotential height field.

Figure 5: First of the 1000-hPa NH (north of 30°N) geopotential height field. Negative values are shaded. The fraction of explained total variance is given at the upper right corner.

Figure 6: First 9 eigenvalues λ_i, together with their error bars, of the covariance matrix between time series of the NH 50 hPa and 500 hPa geopotential heights determined with SVD analysis.
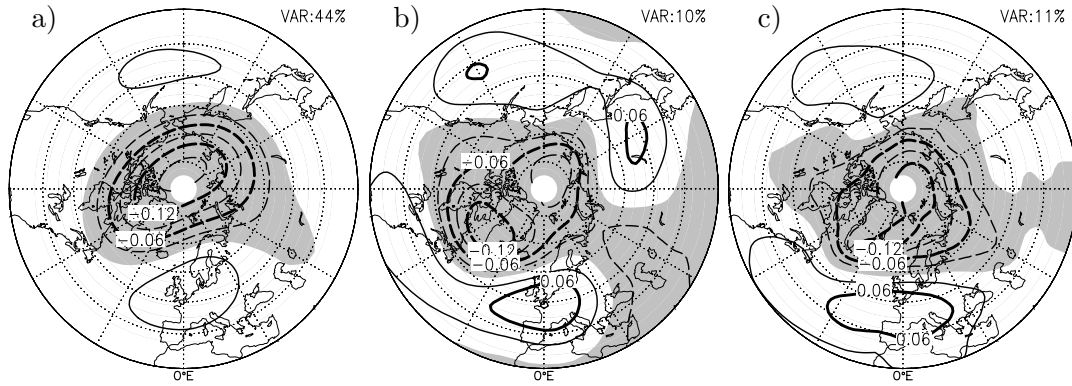
Figure 7: Singular patterns of the first SVD mode determined of the time series of the 50- and 500-hPa geopotential height fields. (a) 50-hPa and (b) 500-hPa geopotential heights. (c) 1000-hPa singular pattern of the first coupled mode in the 50- and 1000-hPa height fields. The fraction of explained total variance is given at the upper right corner of the individual maps.
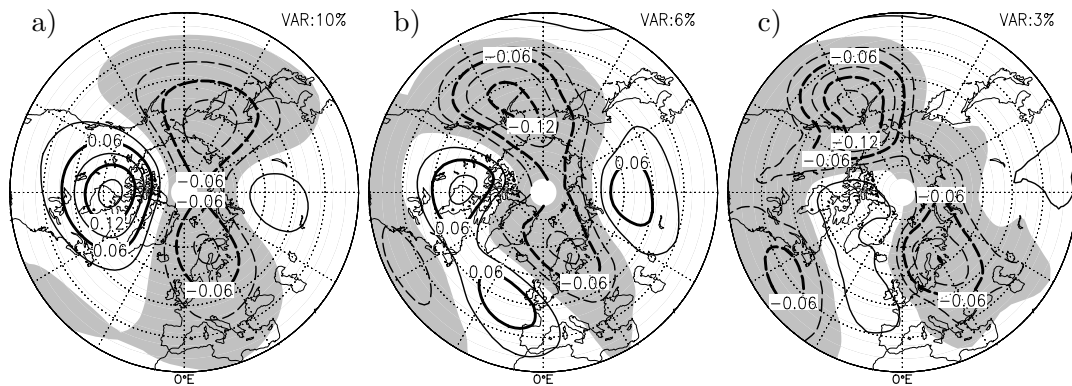

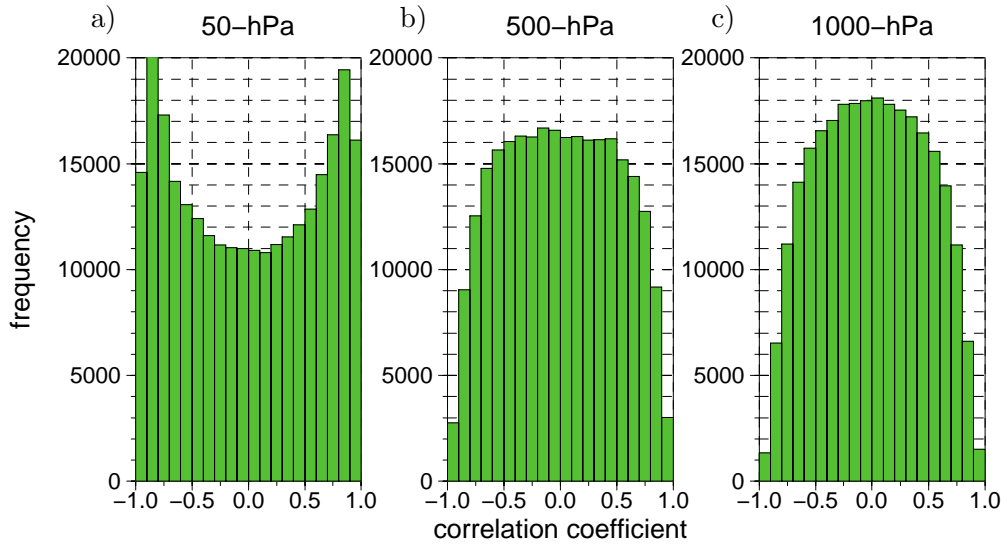Figure 8: Same as Figure 7, but for the second coupled mode.

Figure 9: Frequency distribution of the anomaly correlation r_{ij} between all possible pairs of low-pass filtered anomaly graphs of $\bar{u}$, excluding those from the same winter. a) $\bar{u}_{50}$, b) $\bar{u}_{500}$ and c) $\bar{u}_{1000}$.
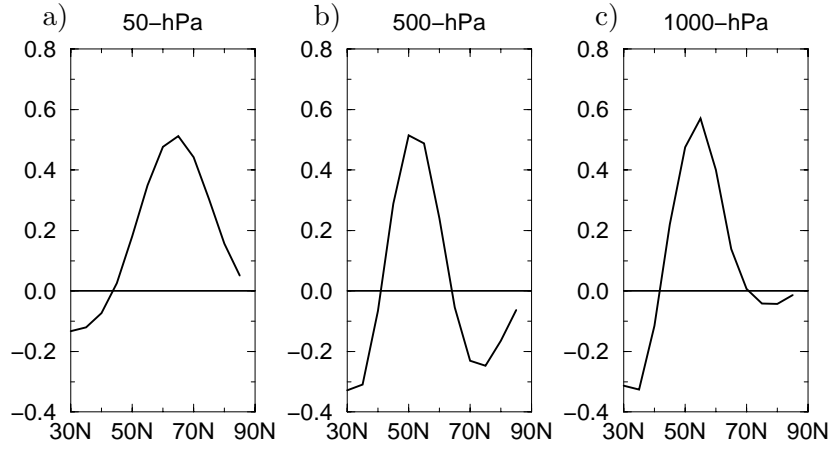

Figure 10: First EOF of zonally-averaged zonal wind during winter, determined on the basis of low-pass filtered daily data. a) 50-hPa level, b) 500-hPa level and c) 1000-hPa level.
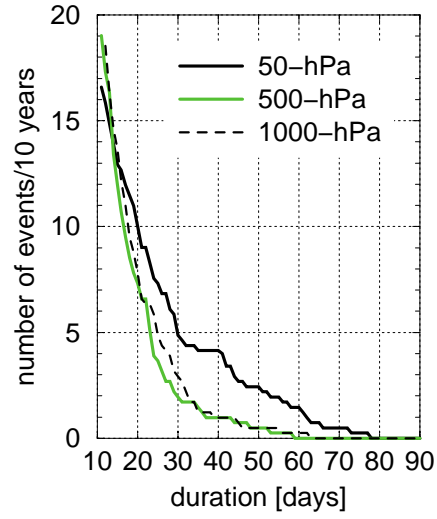
Figure 11: Number of the total sum of events for persistent positive and negative anomalies ($> 0.5\sigma$ or $< -0.5\sigma$), which have the structure of the leading EOF of $\bar{u}$ as a function of the minimum duration exceeded. The distributions are normalized to 10 years. The distributions for the first mode of $\bar{u}$ (north of 30°N) at the 50-, 500- and 1000-hPa level are shown.